Journal of Alloys and Compounds 512 (2012) 270–277

Contents lists available at SciVerse ScienceDirect

Journal of Alloys and Compounds

journal homepage: www.elsevier.com/locate/jallcom

Studying nearest neighbor correlations by atom probe tomography (APT) in metallic glasses as exemplified for $Fe_{40}Ni_{40}B_{20}$ glassy ribbons

Ahmed Shariq[a,b,*], Talaat Al-Kassab[a,c], Reiner Kirchheim[a]

[a] Institute of Material Physics, Georg-August-University, Friedrich-Hund Platz 1, D-37077 Goettingen, Germany
[b] FhG Center Nanoelectronic Technologies, Koenigsbruecker Strasse 180, D-01099 Dresden, Germany
[c] Department of Materials Science & Engineering, King Abdullah University of Science & Technology, Thuwal 23955-6900, Saudi Arabia

ARTICLE INFO

Article history:
Received 5 August 2011
Received in revised form 8 September 2011
Accepted 14 September 2011
Available online 5 October 2011

Keywords:
Atom probe tomography
Data analyses
Metallic glasses
Short range ordering

ABSTRACT

A next nearest neighbor evaluation procedure of atom probe tomography data provides distributions of the distances between atoms. The width of these distributions for metallic glasses studied so far is a few Angstrom reflecting the spatial resolution of the analytical technique. However, fitting Gaussian distributions to the distribution of atomic distances yields average distances with statistical uncertainties of 2 to 3 hundredth of an Angstrom. $Fe_{40}Ni_{40}B_{20}$ metallic glass ribbons are characterized this way in the as quenched state and for a state heat treated at 350 °C for 1 h revealing a change in the structure on the sub-nanometer scale. By applying the statistical tool of the χ^2 test a slight deviation from a random distribution of B-atoms in the as quenched sample is perceived, whereas a pronounced elemental inhomogeneity of boron is detected for the annealed state. In addition, the distance distribution of the first fifteen atomic neighbors is determined by using this algorithm for both annealed and as quenched states. The next neighbor evaluation algorithm evinces a steric periodicity of the atoms when the next neighbor distances are normalized by the first next neighbor distance. A comparison of the nearest neighbor atomic distribution for as quenched and annealed state shows accumulation of Ni and B. Moreover, it also reveals the tendency of Fe and B to move slightly away from each other, an incipient step to Ni rich boride formation.

1. Introduction

The characterization of sub nano-scale transformations, more precisely, short range ordering in metallic glasses was limited because of the resolution limits of many characterization techniques in the past decades. Lewis has though enunciated that the alloys that crystallize initially to a bcc phase e.g. Fe-based alloys, or to an hexagonal close packed (hcp) phase, e.g. Co-based alloys and Ti based metallic glasses, embrittle prior to crystallization [1]. Thus, slight short range rearrangements to incipient bcc or respective groupings may occur in the glassy state, giving rise to embrittlement. For alloys containing high metalloid concentrations segregation of the metalloid(s) may occur, perhaps leading also to the establishment of incipient metal-metalloid groups and/or regions of high concentrations of metalloid(s) which render the alloy brittle. Further, since the metalloid content of glassy alloys clearly determines the mode of crystallization, high metalloid concentrations leading to eutectic or polymorphic crystallization, an alloy of high metalloid content may form incipient groupings involving brittle boride phases that lead to embrittlement.

Different variants of Fe–Ni–B metallic glasses have been studied intensively in the past decades owing to their excellent soft magnetic properties; leading to a number of industrial applications [2]. In addition to their good magnetic properties, a reasonable amount of research is also devoted to mechanical properties of these alloys. Prime interest develops because even slight partial crystallization may end the useful life of the material: palpable loss in high permeability and low coercivity [3,4]. Albeit there is subsequent loss in magnetic properties after annealing, ductile-brittle transition is also reported even for annealing below crystallization temperatures [5–7].

Different rationales include excess free volume that anneals out during annealing thereby making plastic deformation even more difficult alongside the structural relaxation phenomenon upon annealing [8]. Structural relaxation causes a topological change in short range order, i.e., changes in bond distances and bond angles as well as change in chemical short range order, i.e., exchange in chemically different neighbors.

Atom probe tomography provides information in real space on chemical heterogeneities at the atomic scale [9–12]. A specimen

* Corresponding author at: FhG Center Nanoelectronic Technologies, Koenigsbruecker Strasse 180, D-01099 Dresden, Germany. Tel.: +49 351 2607 3060; fax: +49 351 2607 3005.
E-mail address: ahmed.shariq@cnt.fraunhofer.de (A. Shariq).

0925-8388/$ – see front matter © 2011 Elsevier B.V. All rights reserved.
doi:10.1016/j.jallcom.2011.09.079

in the form of a sharp needle is held at cryogenic temperatures in an ultra-high vacuum chamber. Atoms removed as ions from the apex of the specimen by field evaporation are projected onto a position-sensitive detector (PSD). These ions are chemically identified using time-of-flight mass spectrometry. Spatial distribution of different species is revealed from PSD with sub-nanometer lateral resolution, and atomic resolution in depth. Conventionally, different algorithms are applied directly to the 3D reconstructed data to glean direct information about clustering or ordering [13–15]. Moreover, some approaches exclusively deal with pulling out the information about the atomic distance between neighboring atoms of different species [16–18]. In the present study average distances and chemical nature of the next neighbors of all selected atoms are determined for the $Fe_{40}Ni_{40}B_{20}$ metallic glasses in the annealed and in the as prepared state. Using a next nearest neighbor evaluation (NNE) procedure [16], APT experiments divulge all the possible correlations for different elements of the $Fe_{40}Ni_{40}B_{20}$ metallic glasses both for the as quenched state and heat treated state below the crystallization temperature.

2. Methods

The $Fe_{40}Ni_{40}B_{20}$ glassy ribbons are produced by melt spinning in vacuum with a thickness of 30 μm. Sharp needle shape samples for APT studies were produced by first mechanical polishing of the melt spun and heat treated ribbons (1 h at 350 °C) to square shape rods, followed by the electropolishing in a solution of 10% perchloric acid in ethanol. The three dimensional atom probe investigations were performed with a PSD detector [19,20]. During APT analyses, pulse fraction of 20% of the standing voltage were used with a pulse repetition rate of 2000 Hz at a temperature of 30 K. Transmission electron micrographs were utilized to access the details of sample apex geometry for data reconstruction.

The crystallization kinetics was measured by differential scanning calorimetry (DSC) using Perkin Elmer Pyris DSC 7 at a heating rate of 0.33 K/s under an argon gas flow. The diffraction measurements were carried out by X'pert MRD (Philips) with CoKα X-ray source.

2.1. APT data evaluation

χ^2-test was utilized to check homogeneity of the atom probe data, where the analyzed volume is divided into small boxes within which the concentration of the alloying elements is determined. The concentration range of a certain element is split into N appropriate classes and χ^2 is evaluated by the following equation:

$$\chi^2 = \sum_{n=o}^{N} \frac{[F(n) - B(n)]^2}{B(n)} \quad (1)$$

where $F(n)$ is the concentration of an element in class n and $B(n)$ is the corresponding value of the binominal distribution. Then according to Eq. (1), χ^2 is a measure of the deviation of experimentally determined concentration distributions from the binomial or homogeneous one. If this deviation is smaller than values tabulated for a certain significance parameter α, the distribution is called homogeneous. In the present work, $\alpha = 0.05$ was chosen, i.e., for $\chi^2 > \chi^2_\alpha$ the distribution is considered to be homogeneous with an uncertainty of 5%.

A schematic representation for the next nearest neighbor evaluation (NNE) is presented in Fig. 1 for a binary A–B alloy. An arbitrary A-atom is picked as a center atom and distances to the next d_1, second next d_2, and third next A-atom d_3 and so on up to the fifteen next A-atom d_{15} are determined. Then the following A-atom is chosen as the center atom and its distances to the fifteen next A-neighbors are evaluated. After all A-atoms have been chosen as center atoms a distribution of the various A–A distances is obtained as shown for five neighbors in Fig. 2 for the glassy Pd–Cu–P alloy [16]. Analogously, pair distributions of B–B and A–B distances are evaluated. The distributions of atomic distances determined from APT data are convolutions of the resolution function of the atom probe and the actual distributions stemming from the amorphous structure of the samples.

In the context of this paper we are mainly interested in the average values of d_1, d_2, d_3, etc. which will be labeled *NN1*, *NN2*, *NN3*, etc. These average values are determined in this study by fitting Gaussian distributions to the APT data. Thus the mean value of the Gaussian is evaluated and error bars are obtained for this quantity. For all the distributions shown in Fig. 2 and the ones measured in this study the error bars ±0.02 to ±0.03 Å which is about one hundred times less than the width of the distributions.

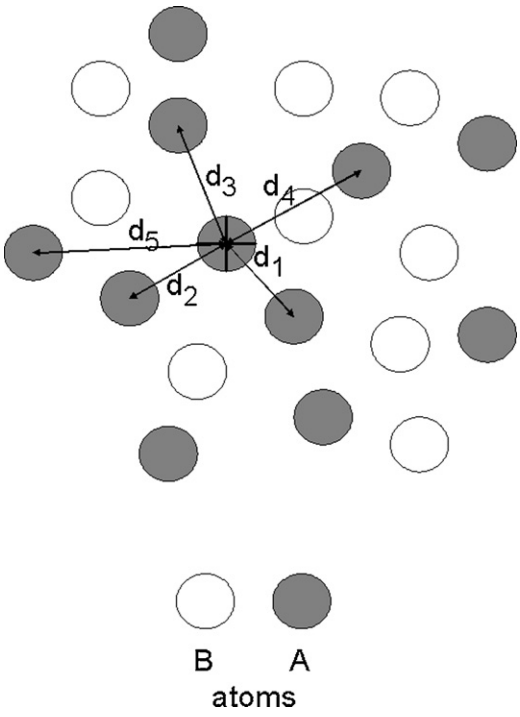

Fig. 1. Schematic presentation of the next neighbor evaluation (NNE) procedure. Distances d_i between B-atoms are monitored starting with the A-atom marked with a cross. First, second, third, ... A-neighbors have the distance d_1, d_2, d_3 and so on. The same procedure is applied for B-atoms and B-neighbors and B-atoms and A-neighbors.

3. Results

The DSC scans of both as quenched and 1 h annealed states of the investigated $Fe_{40}Ni_{40}B_{20}$ metallic glass are shown in Fig. 3. A comparison shows no palpable difference in the heat release of both samples and both DSC scans reveal a pronounced single

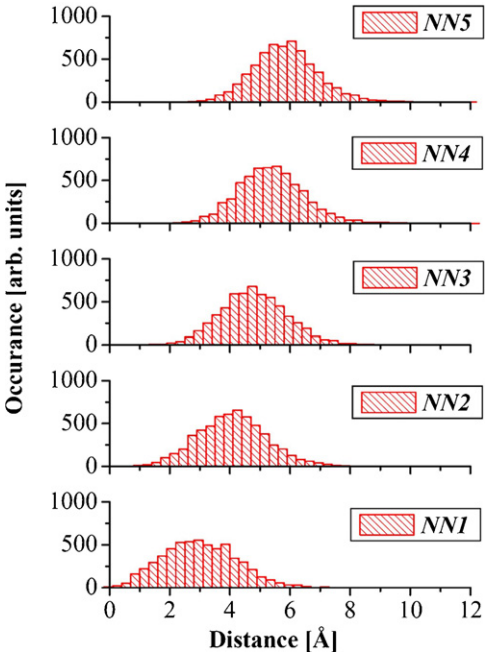

Fig. 2. Histograms calculated using the NNE algorithm for Pd–Cu–P bulk amorphous alloy showing the distance distribution for the first five next neighbors of the Cu–Cu correlation [16].

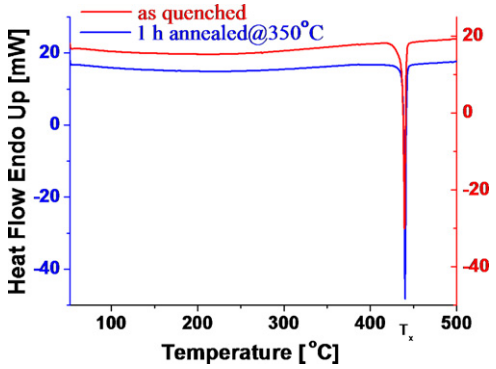

Fig. 3. Comparison of the DSC traces of $Fe_{40}Ni_{40}B_{20}$ metallic glass for as quenched and 1 h annealed at 350 °C, taken at a heating rate of 0.33 K/s.

crystallization peak (T_x) at 440 °C. The DSC scans suggests that there is no major difference in the structure of the as quenched and annealed state. The XRD patterns both for the as quenched and annealed states in Fig. 4 reveal no different results than deduced from the DSC scans. Albeit, first order and second order humps are evident in both patterns, no additional crystallization peaks are featured for the annealed state.

The three dimensional atomic reconstructions of as quenched $Fe_{40}Ni_{40}B_{20}$ glassy ribbon and annealed ribbon are presented in Fig. 5. Visually, both samples exhibit a single homogeneous randomly distributed phase. Fig. 6 represents the three dimensional atomic reconstruction of the individual elements in order to elaborate the stereological representation of atoms for the heat treated samples.

The statistical χ^2 test has been processed to check the homogeneity in both samples. A comparison of the frequency distribution of the experimental data and that from a binomial distribution with the same mean concentration for each constituent of as quenched $Fe_{40}Ni_{40}B_{20}$ glassy ribbons is shown in Fig. 7. For the as quenched sample both the binomial and experimental frequency distributions for Fe and Ni are in general agreement within experimental error. However, very slight hints of deviation between the experimental and binomial distributions of the element boron may be present.

A comparison of the χ^2 values calculated for each constituent element via Eq. (1) and the χ^2 alpha values with 0.05 significance level of alpha, for both as quenched and annealed samples is presented in Table 1. It is evident that the calculated χ^2 values for Fe and Ni are reasonably smaller than χ^2 alpha values, indicating that the Fe and Ni are distributed homogeneously with a probability of 95%. However, for B the calculated χ^2 value exceeds the

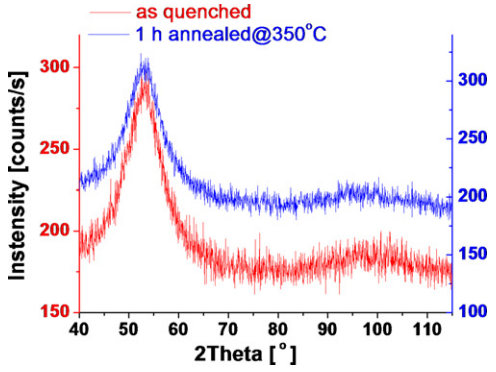

Fig. 4. XRD pattern of as quenched sample and sample annealed for 1 h at 350 °C $Fe_{40}Ni_{40}B_{20}$ metallic glass. Both curves show first order and second order humps typical for amorphous structures.

χ^2 alpha value and therefore, some inhomogeneity may be present for the B distribution. Fig. 8 illustrates a similar comparison of the experimental and binomial distributions for the annealed sample. Subsequent χ^2, χ^2-alpha values and degree of freedom, i.e., *N-1* (cf. Eq. (1)) are also reported in Table 1. The χ^2 values for all elements for the annealed sample exceeds the reference χ^2 alpha values, suggesting inhomogeneous distribution of the constituent elements, especially for the B-distribution for which a pronounced difference is recorded between the two values.

The NNE algorithm is processed to elucidate the fine details related to the short range ordering for both as quenched and annealed $Fe_{40}Ni_{40}B_{20}$ glassy ribbons. The algorithm was processed for a 10 nm × 10 nm × 10 nm volume chosen from the center of the analyzed volume for both as quenched and annealed ribbons. The Gaussian function was fitted for each distribution of *NNs*. The distances of the first fifteen *NNs* for each elemental combination, calculated by processing the aforementioned algorithm on the APT data of as quenched $Fe_{40}Ni_{40}B_{20}$ glassy ribbons are shown in Table 2. The widths obtained were again 2–4 Å and the error bars for the mean distances were in between 0.02 and 0.03 Å. As seen in Table 2 the average distances between an atom and its first, second, third, etc. neighbor of a certain component obey the following relation for all fifteen neighbors

$$\text{Fe–Fe} < \text{Ni–Ni} < \text{Fe–Ni} < \text{Ni–B} < \text{B–B} < \text{Fe–B}$$

Annealing for 1 h at 350 °C does not affect this trend as shown in elemental distribution of *NNs* for annealed $Fe_{40}Ni_{40}B_{20}$ glassy ribbon in Table 3.

4. Discussion

The focus of the present work was utilization of a special algorithm on the APT data to glean out fine details of the atomic structure of a Fe–Ni–B alloy prior to crystallization. Albeit DSC and XRD measurements show no structural differences present in as quenched and annealed $Fe_{40}Ni_{40}B_{20}$ glassy ribbons, APT results depict a change in the structure on the very fine sub-nanometer scale: differences revealed by both χ^2 test and NNE module.

In the as quenched state the χ^2 test reveals a homogeneous distribution of Fe and Ni, whereas the χ^2 value for B is slightly higher than the χ^2 alpha value suggesting that there may be some inhomogeneity present. Nevertheless, this inhomogeneity is more pronounced for the annealed state for B distribution, where a slight deviation from homogeneity is also present for the other constituent elements. This reveals some rearrangement of atoms: an incipient state for the precipitation of a new phase with a different composition when compared with the as prepared alloy.

The NNE module provides information about the atomic distances of the next neighbors for both as quenched and annealed states (Tables 2 and 3). For the as quenched state, the distance of immediate neighboring Fe–Fe, Ni–Ni and B–B pairs are 2.27 Å, 2.56 Å and 2.7 Å, respectively. These values are compared in Table 4 with atomic and covalent diameters (in Å) of each element as reported in the literature. For Fe–Fe and Ni–Ni next neighbors their distances are in same range as atomic and covalent diameters suggesting that these atoms are in mutual contact with each other. However, the separation of B-pairs is much larger than the corresponding diameters and, therefore, suggesting that these atoms are not in contact but separated by either Fe- or Ni-atoms. These values and conclusions are in agreement with the pioneering results obtained by Lamparter and Steeb using neutron scattering for binary amorphous $Fe_{80}B_{20}$ and $Ni_{80}B_{20}$ alloys [21]. A more detailed comparison with diffraction data is provided in the following section.

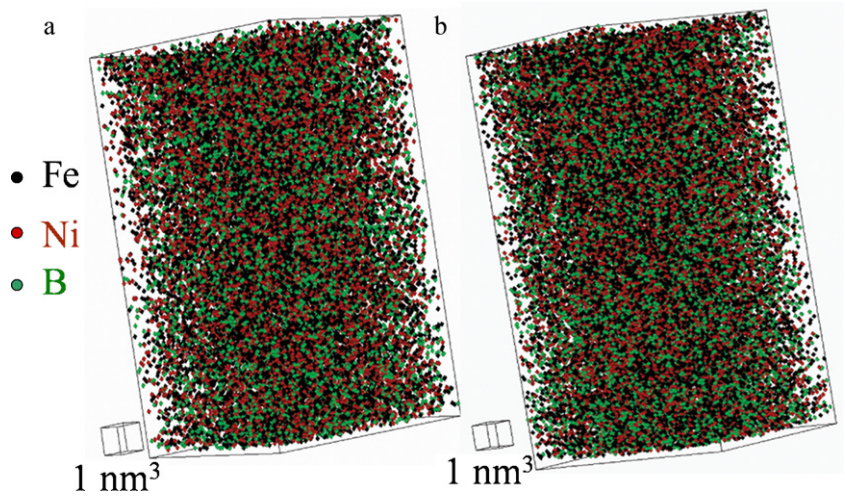

Fig. 5. Three dimensional elemental atomic reconstruction for (a) as quenched and (b) sample annealed for 1 h at 350 °C of the $Fe_{40}Ni_{40}B_{20}$ glassy ribbons. Each dot represents an atomic position of the relative element distinguished by different colors.

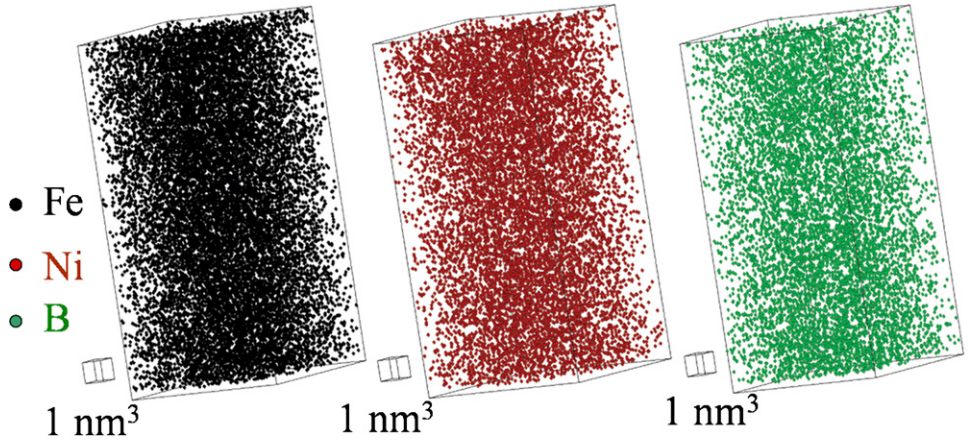

Fig. 6. Three dimensional atomic reconstruction for individual elements for a sample annealed for 1 h at 350 °C of the $Fe_{40}Ni_{40}B_{20}$ glassy ribbons. Each dot represents the atomic position of an alloying element distinguished by different colors.

Table 1
Summary of the calculated χ^2 values for both as quenched and annealed $Fe_{40}Ni_{40}B_{20}$ glassy ribbons. The value of χ^2-alpha for the stated degree of freedom is also given for comparison, with 0.05 significance level of alpha.

$Fe_{40}Ni_{40}B_{20}$	As quenched			1 h @350 °C		
Elements	Fe	Ni	B	Fe	Ni	B
χ^2 (Eq. (1))	27	23	72.4	64.4	84	393.2
χ^2-alpha	45	41	41	45	43	41
DOF (*N-1*)	31	28	28	31	29	28

Table 2
Summary of the average distances of the first fifteen next neighbor atoms for different correlations as calculated by processing the NNE algorithm to APT data for the as quenched $Fe_{40}Ni_{40}B_{20}$ glassy ribbon. The distances are in Å and error bars are between 0.02 and 0.03 Å.

NNi	Fe–Fe	Ni–Ni	Fe–Ni	Ni–B	B–B	Fe–B
NN1	2.27	2.56	2.57	2.65	2.7	2.75
NN2	3.04	3.44	3.45	3.53	3.66	3.67
NN3	3.56	4.02	4.05	4.11	4.29	4.3
NN4	3.96	4.49	4.5	4.58	4.79	4.79
NN5	4.29	4.88	4.89	4.97	5.21	5.21
NN6	4.59	5.22	5.23	5.31	5.57	5.57
NN7	4.85	5.52	5.53	5.61	5.9	5.89
NN8	5.09	5.8	5.8	5.88	6.19	6.18
NN9	5.3	6.05	6.06	6.13	6.47	6.45
NN10	5.51	6.28	6.29	6.37	6.72	6.7
NN11	5.7	6.5	6.51	6.59	6.95	6.93
NN12	5.87	6.7	6.72	6.79	7.17	7.15
NN13	6.04	6.9	6.91	6.99	7.38	7.36
NN14	6.21	7.09	7.1	7.17	7.57	7.56
NN15	6.36	7.26	7.28	7.35	7.76	7.75

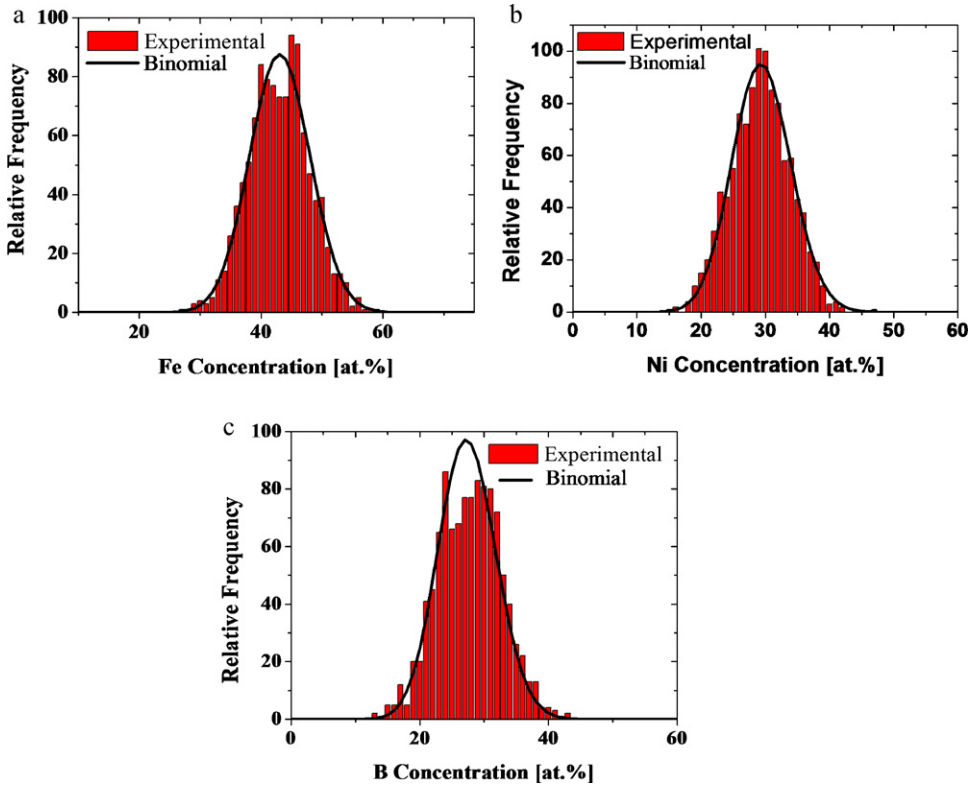

Fig. 7. Comparison of the experimental frequency distribution to the binomial distribution of the same concentration for as quenched $Fe_{40}Ni_{40}B_{20}$ glassy ribbon sample. The illustrated distributions are for all the constituent elements, i.e., (a) Fe, (b) Ni and (c) B.

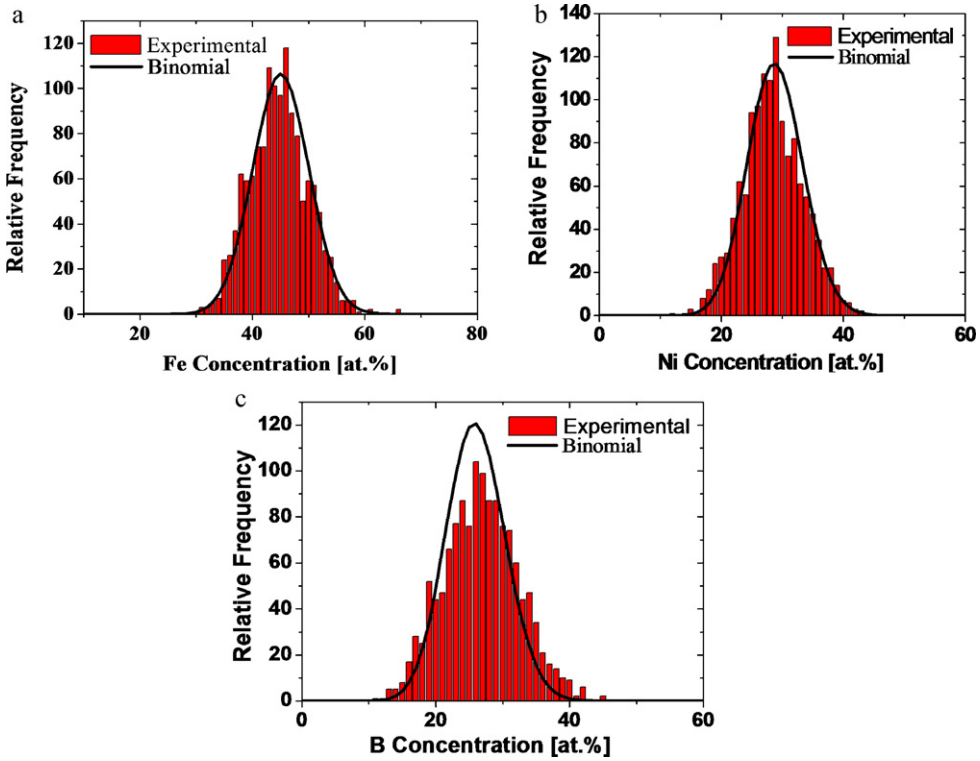

Fig. 8. Comparison of the experimental frequency distribution to the binomial distribution of the same concentration for $Fe_{40}Ni_{40}B_{20}$ glassy ribbon annealed 1 h at 350 °C. The illustrated distributions are for all the constituent elements, i.e., (a) Fe, (b) Ni and (c) B.

Table 3
Summary of the average distances of the first fifteen next neighbor atoms for different correlations as calculated by processing the NNE algorithm to TAP data for the $Fe_{40}Ni_{40}B_{20}$ glassy ribbon annealed for 1 h at 350 °C. The distances are in Å and error bars are between 0.02 and 0.03 Å.

NNi	Fe–Fe	Ni–Ni	Fe–Ni	Ni–B	B–B	Fe–B
NN1	2.18	2.5	2.52	2.55	2.68	2.79
NN2	2.92	3.37	3.39	3.42	3.65	3.7
NN3	3.42	3.95	3.97	4.02	4.28	4.33
NN4	3.82	4.41	4.43	4.48	4.77	4.83
NN5	4.14	4.79	4.8	4.86	5.19	5.24
NN6	4.43	5.12	5.13	5.19	5.54	5.59
NN7	4.68	5.42	5.43	5.48	5.86	5.91
NN8	4.91	5.69	5.69	5.76	6.15	6.2
NN9	5.12	5.93	5.94	6	6.42	6.46
NN10	5.31	6.16	6.16	6.23	6.68	6.71
NN11	5.49	6.38	6.38	6.44	6.91	6.95
NN12	5.66	6.58	6.58	6.65	7.14	7.17
NN13	5.82	6.77	6.77	6.84	7.35	7.37
NN14	5.98	6.95	6.95	7.02	7.54	7.57
NN15	6.12	7.12	7.12	7.19	7.73	7.76

4.1. Comparison with earlier investigations

Sietsma and Thijsse published for the $Fe_{40}Ni_{40}B_{20}$ metallic glass three partial reduced radial distribution functions as obtained by neutron diffraction experiments [22]. The three partial RDFs were calculated by applying isotopic substitution from $Fe_{40}Ni_{40}{}^{11}B_{20}$, $Fe_{40}{}^{60}Ni_{40}{}^{11}B_{20}$, $Fe_{40}{}^{62}Ni_{40}{}^{11}B_{20}$ samples [23]. Moreover, for the calculations it was assumed that the following relation for the Fe–Fe and Ni–Ni structure factor is obeyed $S_{FeFe}(Q) = S_{NiNi}(Q)$. Peak positions of the coordination shells for three partial reduced radial distribution functions, i.e., for Fe–Fe, Ni–Ni (denoted as MM), Fe–Ni, and Fe–B, Ni–B (denoted as MB) from Sietsma's work [22] and the results from the present study (as quenched state) are summarized in Table 5. The plausible methodology adapted for a comparison with the reduced radial distribution function calculated from the scattering techniques, is to take the average of *NN*s having the same distance range as that of the corresponding coordination peak/sub peak. For example, for Fe–Ni correlation, only *NN1* has comparable distance to that of the first peak in the corresponding PRDF (r_1^1) [22], hence considered. Subsequently, *NN2–NN4* corresponds to the sub-peak1 of the second peak in the corresponding PRDF (i.e., r_2^1) and hence averaged.

Deduced values PRDF estimates from the present study corroborate reasonably with the results from Sietsma and Thijsse. It should be noted that they found for the transition metal-metalloid (Fe–B, Ni–B) correlation a first coordination peak with two sub peaks. However, the present NNE results do not show a metal–metalloid distance corresponding to the first sub peak but lie in the range of the second sub-peak. It is worth mentioning that utilizing APT, it is possible to reveal all different elemental correlations regardless of the number of the constituent elements which is quite improbable to be evaluated unambiguously from diffraction data.

4.2. Comparison between quenched and annealed states

To elaborate changing atom distances between the as quenched and annealed states of the $Fe_{40}Ni_{40}B_{20}$ glassy ribbon, differences between corresponding elemental correlations are presented in Table 6. For all correlations except that of Fe–B positive values were obtained corresponding to a decrease of the distances between all atoms. This is in agreement with the expectation, because the annealed samples are believed to represent a more relaxed structure with decreased atomic distances. It should be noted that these differences are equal or larger than the error bars of the mean value of fitted Gaussians.

The magnitude of changes for different elemental correlations upon annealing follows the sequence as under:

$$\text{Fe–B} < \text{B–B} < \text{Ni–Ni} < \text{Fe–Ni} < \text{Ni–B} < \text{Fe–Fe}$$

It shows that for the annealed state Fe–B has a slight tendency to move away from each other, contrary to the Ni–B which are attracted to each other. It evinces that the Ni boride is more favorable than Fe boride. Gibb's free energies of both borides at 327 °C are considered and given as under

Ni_4B_3	−397.87 kJ/mol [24]
NiB	−123.25 kJ/mol [24]
FeB	−98.73 kJ/mol [25]

Lucidly, the Gibbs free energy for Nickel boride formation being more negative than that of the Iron boride gives a plausible explanation for the tendency of B to move towards the Ni.

Different stages of crystallization had earlier been investigated by Mitra et al. X-ray diffraction data from their study revealed early stages (though at higher temperature, i.e., 457 °C) of crystallization of a solid solution of FeNi alongside the compounds $Fe_{4.5}Ni_{18.5}B_6$ and Ni_4B_3 [26]. Further crystallization leads to the formation of Ni_4B_3, $Fe_{4.5}Ni_{18.5}B_6$ and Fe_3Ni_3B borides.

The results of the present study reveal the tendency of the incipient grouping of Ni and B that may be either directly to yield the aforementioned Ni rich boride, i.e., Ni_4B_3 or a step towards the formation of ternary Ni-rich $Fe_{4.5}Ni_{18.5}B_6$. For the formation of the $Fe_{4.5}Ni_{18.5}B_6$, boron atoms have to move away from the Fe and towards the Ni to meet the required stoichiometry. It also corroborates the theory proposed by Lewis that slight short range rearrangements for alloys containing high metalloid concentrations may occur by segregation of the metalloid(s), perhaps leading also to the establishment of incipient metal–metalloid groups and/or regions of high concentrations of metalloid(s) which render the alloy brittle.

4.3. Steric periodicity of atomic distribution

To elaborate any structural periodicity, the distance of the each *NN* is divided by the first *NN* of the corresponding correlation and compiled in Table 7. The normalized distances of each correlation seem to be independent of the chemical identity. For a

Table 4
Next neighbor distances *NN1* for the as quenched state and atomic and covalent diameters of the corresponding elements.

Pair of elements	Next neighbor distance *NN1* (Å)	Atomic diameter (Å)	Covalent diameter (Å)
Fe–Fe	2.27	2.52	2.34
Ni–Ni	2.56	2.48	2.30
B–B	2.7	1.96	1.64

Table 5
Summary of the distances of the first (r^1) and second (r^2) peak position of the coordination shells of the partial reduced radial distribution functions for $Fe_{40}Ni_{40}B_{20}$ metallic glasses [22] and a comparison with the results of the present study by applying the NNE module for the as quenched state. Distances are given in Å and subpeaks are denoted by subscripts.

	$Fe_{40}Ni_{40}B_{20}$ (Sietsma and Thijsse [22])			$Fe_{40}Ni_{40}B_{20}$ (Present work)				
	M–M	Fe–Ni	M–B	Fe–Fe	Ni–Ni	Fe–Ni	Ni–B	Fe–B
r_1^1	2.52	2.53	2.15	2.66	2.56	2.57	2.65	2.75
r_2^1			2.83					
r_1^2	4.23	4.18	4.34	4.1	3.98	4	4.3	4.25
r_2^2	4.85	4.85		4.97	5.05	5.06		

Table 6
Differences in Å for the average distances of first fifteen next neighbor atoms between the as quenched and annealed states of $Fe_{40}Ni_{40}B_{20}$ glassy ribbons (q denotes as quenched and a denotes annealed state).

	Fe–B	B–B	Fe–Ni	Ni–Ni	Fe–Fe	Ni–B
$NN1_q$–$NN1_a$	−0.04	0.02	0.05	0.06	0.09	0.1
$NN2_q$–$NN2_a$	−0.03	0.01	0.06	0.07	0.12	0.11
$NN3_q$–$NN3_a$	−0.03	0.01	0.08	0.07	0.14	0.09
$NN4_q$–$NN4_a$	−0.04	0.02	0.07	0.08	0.14	0.1
$NN5_q$–$NN5_a$	−0.03	0.02	0.09	0.09	0.15	0.11
$NN6_q$–$NN6_a$	−0.02	0.03	0.1	0.1	0.16	0.12
$NN7_q$–$NN7_a$	−0.02	0.04	0.1	0.1	0.17	0.13
$NN8_q$–$NN8_a$	−0.02	0.04	0.11	0.11	0.18	0.12
$NN9_q$–$NN9_a$	−0.01	0.05	0.12	0.12	0.18	0.13
$NN10_q$–$NN10_a$	−0.01	0.04	0.13	0.12	0.2	0.14
$NN11_q$–$NN11_a$	−0.02	0.04	0.13	0.12	0.21	0.15
$NN12_q$–$NN12_a$	−0.02	0.03	0.14	0.12	0.21	0.14
$NN13_q$–$NN13_a$	−0.01	0.03	0.14	0.13	0.22	0.15
$NN14_q$–$NN14_a$	−0.01	0.03	0.15	0.14	0.23	0.15
$NN15_q$–$NN15_a$	−0.01	0.03	0.16	0.14	0.24	0.16

Table 7
The ratio for different elemental correlations after normalizing the average distances of the first fifteen next neighbors by the average distance of first neighboring atom for the as quenched state. Averaged normalized ratios for the annealed state are also given for a comparison. The distances are in Å.

	Fe–Fe	Ni–Ni	Fe–Ni	B–B	Fe–B	Ni–B	Average as quenched	Average annealed
NN2/NN1	1.34	1.35	1.34	1.36	1.33	1.34	1.34 ± 0.02	1.35 ± 0.02
NN3/NN1	1.57	1.58	1.57	1.6	1.56	1.56	1.56 ± 0.03	1.58 ± 0.03
NN4/NN1	1.75	1.76	1.75	1.78	1.74	1.74	1.74 ± 0.03	1.76 ± 0.03
NN5/NN1	1.89	1.91	1.9	1.94	1.89	1.88	1.88 ± 0.04	1.91 ± 0.04
NN6/NN1	2.02	2.04	2.03	2.07	2.02	2.02	2.02 ± 0.04	2.04 ± 0.05
NN7/NN1	2.14	2.16	2.15	2.19	2.14	2.13	2.13 ± 0.04	2.16 ± 0.05
NN8/NN1	2.24	2.27	2.26	2.3	2.24	2.23	2.23 ± 0.05	2.26 ± 0.05
NN9/NN1	2.34	2.37	2.36	2.4	2.34	2.33	2.33 ± 0.05	2.36 ± 0.05
NN10/NN1	2.43	2.46	2.45	2.5	2.43	2.42	2.42 ± 0.06	2.45 ± 0.05
NN11/NN1	2.51	2.55	2.53	2.58	2.51	2.5	2.5 ± 0.06	2.53 ± 0.06
NN12/NN1	2.59	2.63	2.61	2.66	2.59	2.58	2.58 ± 0.06	2.61 ± 0.06
NN13/NN1	2.66	2.71	2.69	2.74	2.67	2.65	2.65 ± 0.07	2.69 ± 0.07
NN14/NN1	2.74	2.78	2.76	2.81	2.74	2.72	2.72 ± 0.07	2.76 ± 0.07
NN15/NN1	2.8	2.85	2.83	2.88	2.81	2.79	2.79 ± 0.07	2.83 ± 0.07

comparison, the average normalized ratios of the *NN*s of the annealed samples are also presented here. The resultant normalized ratios are somewhat identical for all elemental correlations independent of chemical nature. Such an atomic periodicity independent of the elemental correlation, reveals that the underlying principle responsible for periodicity is rather steric: the arrangement of atoms according to the constraint of filling the three dimensional space contrary to the one suggested by Häussler [27]. Intriguingly, the same findings have already been reported for Pd based amorphous alloys [16].

5. Conclusions

XRD and DSC, the conventional characterization tools do not show any structural transformation for 1 h annealed $Fe_{40}Ni_{40}B_{20}$ metallic glass at 350 °C. APT results, however, depict a change in the structure on the very fine sub-nanometer scale. Albeit, χ^2 test reveals pronounced inhomogeneity for the annealed state, there were slight hints of inhomogeneity for B distribution even for the as quenched $Fe_{40}Ni_{40}B_{20}$ glassy ribbon.

The NNE algorithm presented in this study successfully allows the evaluation of the first fifteen next neighbors for both as quenched and annealed states. The distances for the next neighbors of different elemental correlations are in a good agreement with the data available in the literature. The distance distributions of next neighboring atoms show that Fe–Fe atoms have the highest probability to be the next neighbors to each other. A steric periodicity of the atoms is also depicted by normalizing the *NN* distances by the first next neighbor distance *NN1*; yielding a ratio similar for all elemental correlations proves that there exists a certain order among the atoms, irrespective of their chemical nature. A comparison of the *NN* atomic distribution for as quenched and annealed states reveals accumulation of Ni and B. It also shows the tendency of Fe and B to move slightly away from each other. These findings

are in good agreement with the Gibbs free energies for Ni- and Fe boride formation; a Ni rich boride formation is also enunciated by Mitra et al. [26]. The tendency of incipient grouping corroborates Lewis's postulate about the changes in short range ordering, a primordial step to boride formation, which causes embrittlement of the $Fe_{40}Ni_{40}B_{20}$ metallic glass even before the crystallization temperature.

Acknowledgement

The Lower Saxony's government and SFB 602 are gratefully acknowledged for the financial support of this project.

References

[1] B.G. Lewis, H.A. Davies, K.D. Ward, Scripta Metall. 13 (1979) 313.
[2] F.E. Luborsky, Ferromagnetic Materials, Wohlfarth P, N-H, Amsterdam, 1980.
[3] J.L. Walter, F.E. Luborsky, Mater. Sci. Eng. 33 (1978) 91.
[4] A.L. Greer, Acta Metall. 30 (1982) 171.
[5] H.S. Chen, Mater. Sci. Eng. 26 (1976) 79.
[6] M.F. Ashby, A.L. Greer, Scripta Mater. 54 (2006) 321.
[7] J. Piller, P. Haasen, Acta Metall. 30 (1982) 1.
[8] J. Li, Metallic Glasses, ASM, Metals Park, Ohio, 1977, 224.
[9] M. Oehring, P. Hassen, J. Phys. 47-C7 (1986) 275.
[10] M.P. Macht, N. Wanderka, A. Wiedenmann, H. Wollenberger, Q. Wei, H.J. Fecht, S.G. Klose, Mater. Sci. Forum 65 (1996) 225.
[11] M.K. Miller, Mater. Sci. Eng. A 250 (1998) 133.
[12] R. Busch, S. Schneider, A. Peker, W.L. Johnson, Appl. Phys. Lett. 67 (1995) 1544.
[13] A. Heinrich, T. Al-Kassab, R. Kirchheim, Mater. Sci. Eng. A 353 (2002) 92.
[14] J.M. Hyde, A. Cerezo, T.J. Williams, Ultramicroscopy 109 (2009) 502.
[15] C.K. Sudbrack, R.D. Noebe, D.N. Seidman, Phys. Rev. B 73 (2006) 4.
[16] A. Shariq, T. Al-Kassab, R. Kirchheim, R.B. Schwarz, Ultramicroscopy 107 (2007) 773.
[17] B.P. Geiser, T.F. Kelly, D.J. Larson, J. Schneir, J.P. Roberts, Microsc. Microanal. 13 (2007) 437.
[18] L.T. Stephenson, M.P. Moody, P.V. Liddicoat, S. Ringer, Microsc. Microanal. 13 (2007) 448.
[19] D. Blavette, B. Deconihout, A. Bostel, J.M. Sarrau, M. Bouet, A. Menand, Rev. Sci. Instrum. 64 (1993) 2911.
[20] T. Al-Kassab, H. Wollenberger, G. Schmitz, R. Kirchheim, F. Ernst, M. Rühle (Eds.), High Resolution Imaging and Spectrometry of Materials, Springer Series of Material Science, Springer, Berlin, Heidelberg, 2003, p. 274.
[21] P. Lamparter, S. Steeb, in: R.W. Cahn, P. Haasen, E.J. Kramer (Eds.), Materials Science and Technology, vol. 1, 1993, p. 236.
[22] J. Sietsma, B.J. Thijsse, J. Phys. F: Met. Phys. 17 (1987) 1.
[23] C.N.J. Wagner, D. Lee, J. Phys. Coll. 41-C8 (1980) 242.
[24] I. Barin, Thermochemical Data of Pure Substances, second ed., VCH Verlagsgesellschaft, Weinheim, 1993, p. 1056.
[25] I. Barin, Thermochemical Data of Pure Substances, second ed., VCH Verlagsgesellschaft, Weinheim, 1993, p. 539.
[26] A. Mitra, S. Rao, S. Pramanik, O.N. Mohanty, J. Mat. Sci. 27 (1992) 5863.
[27] P. Häussler, J. Phys. (Paris) C8 (1985) 361.